cSupporting Information

Qiang, et al. 10.1073/pnas.0907360106

SI Text

Synthesis of 5-^{19}F-DPPC

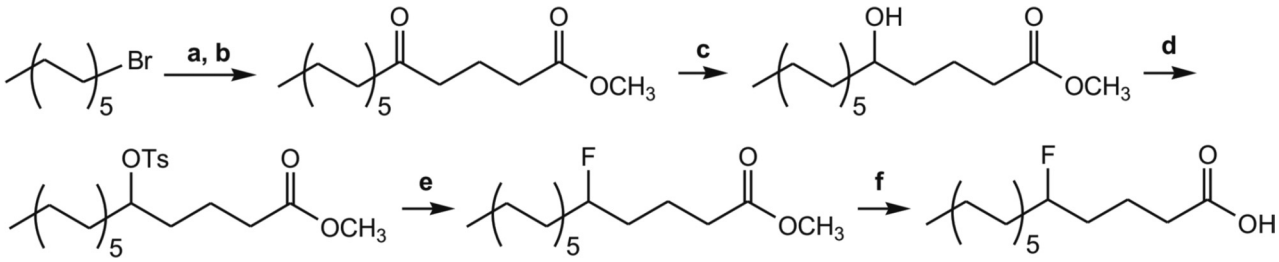

Scheme 1. Synthesis of 5-^{19}F-palmitic acid.

Scheme S1 summarizes the synthesis of 5-^{19}F-palmitic acid which was used to make 1-palmitoyl-2-(5-fluoropalmitoyl)-*sn*-glycero-3-phosphocholine (5-^{19}F-DPPC) (1–5). The overall yield of 5-^{19}F-palmitic acid was ≈40% and each step was monitored by using thin layer chromatography with iodine and phosphomolybdic acid as visualization reagents. The intermediate products were purified by using silica gel column chromatography with a mixture of pentane and ethyl acetate as developing solutions. The 5-^{19}F-DPPC was synthesized by Avanti Polar Lipids.

Reaction conditions in Scheme S1 included: (*i*) 68.2 g of undecyl bromide in 350 mL of dry diethyl ether was added to 6.94 g Mg in 100 mL of dry diethyl ether. Reflux at 34 °C for 2 h. (*ii*) The diethyl ether was removed and 28.0 g of methyl 4-(chloro-formyl) butyrate in 100 mL of dry benzene was added to the Grignard solution from step a and 27.5 g of $CdCl_2$ in 350 mL of dry benzene. Reflux at 78 °C for 1 h. (*iii*) $NaBH_4$, NaH_2PO_4 and 5-keto-methyl palmitate each at 1 M concentration were dissolved in dry methanol. The mixture was stirred at 0 °C for 15 min and at ambient temperature for 1 h. (*iv*) 5-hydroxy-methyl palmitate and 0.5 M tosyl chloride each at 0.5 M concentration were dissolved in dry CH_2Cl_2 with 0.025 M 4-(dimethylamino)pyridine. The mixture was cooled and held at 0 °C, dry pyridine was added dropwise >40 min to reach a final concentration 0.5 M, and then the mixture was stirred at 0 °C for 2 h. (*v*) 0.05 M 5-O-tosyl-methyl palmitate and 0.1 M tetrabutylammonium fluoride in dry CH_3CN were stirred at ambient temperature for 96 h. (*vi*) 5-F-methyl palmitate and KOH powder were each added into dry methanol at 0 °C to reach a final concentration of 0.1 M of each reagent. The mixture was stirred at 0 °C for 2 h.

Sample Preparation. HFPmn and HFPmn_mut were synthesized manually by using Fmoc chemistry. HFPtr was synthesized by using a Cys cross-linking reaction between monomer and dimer building blocks (6). In Table 1, the residues that are C-terminal of Ser-23 are nonnative and act as 280 nm chromophores for HFP quantitation (W), improve aqueous solubility (K), or are used for cross-linking (K and C). The line between K and C denotes a peptide bond between the Cys carbonyl and the Lys ε-NH and a line between two Cs denotes a disulfide bond. All peptides were purified by using reverse-phase HPLC with a H_2O-CH_3CN gradient containing 0.1% TFA and identified with MALDI-TOF mass spectrometry. Membrane preparation began with dissolution in chloroform of a mixture of 16 μmol DTPC, 4 μmol DTPG, 2 μmol 16-^{19}F-DPPC (purchased from Avanti Polar Lipids) or 5-^{19}F-DPPC, and 10 μmol cholesterol. The chloroform was removed under a stream of nitrogen followed by overnight vacuum pumping. The lipid film was suspended in 2 mL of 5 mM *N*-(2-hydroxy-ethyl)piperazine-*N*′-2-ethanesulfonic acid (Hepes) buffer with pH = 7.0 and 0.01% NaN_3 and homogenized with 10 freeze-thaw cycles. Large unilamellar vesicles were formed by extrusion through a polycarbonate filter with 100-nm diameter pores (Avestin). HFPmn or HFPmn_mut (0.8 μmol) or HFPtr (0.27 μmol) (as determined by using ε_{280} = 5700 cm^{-1} M^{-1} for HFPmn_mut and HFPmn or ε_{280} = 17100 cm^{-1} M^{-1} for HFPtr) was dissolved in 2 mL of Hepes buffer, and the HFP and vesicle solutions were then gently vortexed together overnight. The mixture was ultracentrifuged at ≈150,000 × *g* for 5 h. The membrane pellet with associated bound HFP was transferred to a 4-mm diameter NMR rotor. Unbound HFP does not pellet under similar conditions (7).

Solid-State NMR Spectroscopy. Experiments were conducted on a 9.4 T solid-state NMR spectrometer (Varian Infinity Plus) with a quadruple-resonance magic angle spinning (MAS) probe equipped for 4-mm diameter rotors and tuned to ^{1}H, ^{13}C, ^{31}P, and ^{19}F nuclei. The ^{13}C shifts were externally referenced to the methylene resonance of adamantane at 40.5 ppm. The REDOR experiments were done by using a pulse sequence in which the dephasing period had one ^{13}C π pulse per rotor cycle for the S_0 and S_1 acquisitions and one ^{31}P or ^{19}F π pulse per rotor cycle for the S_1 acquisition (8). The dephasing period of the S_0 acquisition did not contain the ^{31}P or ^{19}F π pulses. Experimental parameters included: 8.0 kHz MAS frequency; 50 kHz ^{1}H $\pi/2$ pulse; 50 kHz ^{1}H and 55–66 kHz ramped ^{13}C fields during 1-ms cross polarization; 50 kHz ^{13}C and 50 kHz ^{31}P or 33 kHz ^{19}F π pulses during the dephasing period; 95 kHz ^{1}H decoupling during the dephasing and acquisition periods; and 1-s recycle delay. Most of the setup of the NMR experiments was the same as described in earlier studies and included calibration of the ^{1}H, ^{13}C, and ^{31}P rf fields (6, 8). Nitrogen gas cooled to −50 °C was flowed over the sample to enhance signal-to-noise but this sample cooling does not affect HFP conformation (9). There is also no phase transition of the cholesterol-rich membranes between ambient and low temperature (10).

After acquisition of the REDOR NMR data, a 1 ppm region around the peak chemical shift of each S_0 and S_1 spectrum was integrated, and the integration values were denoted as S_0^{exp} and S_1^{exp}. The experimental normalized dephasing $(\Delta S/S_0)^{exp} = (S_0^{exp} - S_1^{exp})/S_0^{exp}$.

The ^{13}CO-^{19}F experiments were validated by using a lyophilized sample containing helical peptide F whose sequence EQLLKALEFLLKELLEKL was modified by substitution of Phe-9 with *p*-fluorophenylalanine (11). A ^{13}CO label was placed at Leu-10 and the REDOR-determined ^{13}CO-^{19}F distance was 7.8 Å and correlated with the 7.1-Å distance between the Leu-10 carbonyl carbon and the Phe-9 aromatic C4 carbon in the crystal structure of nonfluorinated peptide F.

Effect of mol Fraction Fluorinated Lipid on $(\Delta S/S_0)^{exp}$. A 100% 16-^{19}F-DPPC lipid sample forms a nonbilayer structure (12). To maintain bilayer structure in the NMR samples, the membrane composition was 16 μmol DTPC, 4 μmol DTPG, 10 μmol cholesterol, and 2 μmol ^{19}F-DPPC. This 0.09 lipid mol fraction of ^{19}F-DPPC was initially determined with measurements on a series of samples which differed in their mol fraction of 5-^{19}F-DPPC (Fig. S1). The choice of 0.09 mol fraction ^{19}F-DPPC for subsequent samples was based on: (*i*) maximum ^{13}CO-^{19}F $(\Delta S/S_0)^{exp}$; and (*ii*) relatively constant $(\Delta S/S_0)^{exp}$ over the 0.07–0.14 mol fraction range. Static ^{31}P NMR spectra were consistent with overall bilayer structure in samples containing 0.09 mol fraction 5-^{19}F-DPPC and HFPs (13).

Calculation of $(\Delta S/S_0)^{lab}$. Removal of the natural abundance ^{13}CO contribution to $(\Delta S/S_0)^{exp}$ resulted in $(\Delta S/S_0)^{lab}$ which reflected the labeled ^{13}CO contribution to the experimental data. The experimental ^{13}CO signals have three contributions: (1) labeled ^{13}COs; (2) natural abundance HFP ^{13}COs; and (3) natural abundance ^{13}COs of the ^{19}F-DPPC lipid. In each sample, the labeled S_0 ^{13}CO contribution is assigned a value of 1, the fractional ^{13}C natural abundance is 0.011, the ratio of unlabeled to labeled HFP residues is ≈29, and the ^{19}F-DPPC:HFP strand mol ratio is ≈2.5 with two COs per ^{19}F-DPPC.

$$S_0^{exp} = S_0^{lab} + S_0^{na}(HFP) + S_0^{na}(DPPC) = 1 + (29 \times 0.011) + (2.5 \times 2 \times 0.011) = 1.374 \quad \textbf{[S1]}$$

$$S_1^{exp} = S_1^{lab} + S_1^{na}(HFP) + S_1^{na}(DPPC) \quad \textbf{[S2]}$$

$$S_1^{na}(HFP) = S_0^{na}(HFP) \times g^{na}(HFP) \quad \textbf{[S3a]}$$

$$S_1^{na}(DPPC) = S_0^{na}(DPPC) \times g^{na}(DPPC) \quad \textbf{[S3b]}$$

Calculation of the $g^{na}(HFP)$ and $g^{na}(DPPC)$ are discussed in the next paragraph. Algebraic manipulation of Eqs. **S1–S3** yields:

$$\left(\frac{\Delta S}{S_0}\right)^{exp} = \frac{S_0^{exp} - S_1^{exp}}{S_0^{exp}} = \frac{1.374 - S_1^{lab} - [0.319 \times g^{na}(HFP)] - [0.055 \times g^{na}(DPPC)]}{1.374} \quad \textbf{[S4]}$$

$$\left(\frac{\Delta S}{S_0}\right)^{lab} = \frac{S_0^{lab} - S_1^{lab}}{S_0^{lab}} = \left[1.374 \times \left(\frac{\Delta S}{S_0}\right)^{exp}\right] + [0.319 \times g^{na}(HFP)] + [0.055 \times g^{na}(DPPC)] - 0.374 \quad \textbf{[S5]}$$

The $g^{na}(HFP)$ for each construct, dephasing time τ, and lipid nucleus type, i.e., ^{31}P, 16-^{19}F, or 5-^{19}F, was approximated as the average of the $(S_1/S_0)^{exp}$ of all samples with these same parameters. This approximation considers that the HFP ^{13}COs contribute ≈96% of the S_0 signal (Eq. **S1**) and assumes that the distribution of membrane locations of the labeled ^{13}CO sites is reflective of the average membrane location of the HFP. The $g^{na}(DPPC)$ for each τ and lipid nucleus type was approximated as the $(S_1/S_0)^{sim}$ value of a single ^{13}CO-^{31}P or ^{13}CO-^{19}F spin pair with details of the $(S_1/S_0)^{sim}$ calculations given in the next section. The $(S_1/S_0)^{sim}$ depends on internuclear distance and the ^{13}CO-^{31}P distance was set to 5.6 Å which is the experimentally derived average (lipid ^{13}CO)-^{31}P distance in a sample containing DPPC lipid and unlabeled HFPmn (8). The ^{13}CO-(16-^{19}F) and ^{13}CO-(5-^{19}F) distances were 5.6 Å and 15.2 Å, respectively, and were derived from a computational structure of gel phase DPPC (14). The $g^{na}(HFP)$ and $g^{na}(DPPC)$ are presented in Table S2 and Table S3.

Fitting of $(\Delta S/S_0)^{lab}$. For samples with significant nonzero $(\Delta S/S_0)^{lab}$, fitting was done with a model of two types of ^{13}CO-^{31}P or ^{13}CO-^{19}F spin pairs. One type had fractional population f and the other had population $1 - f$. The magnitude of dipolar coupling d was fitted for the f population and was set to 0 for the $1 - f$ population. The $1 - f$ population was included because many of the samples had $(\Delta S/S_0)^{lab} < 1$ at large τ. The $(\Delta S/S_0)^{lab}$ were compared with:

$$\left[\left(\frac{\Delta S}{S_0}\right)(d, \tau)\right]^{sim} = \left\{1 - [J_0(\sqrt{2}d\tau)]^2 + \left[2 \times \sum_{k=1}^{5} \frac{[J_k(\sqrt{2}d\tau)]^2}{16k^2 - 1}\right]\right\} \quad \textbf{[S6]}$$

using:

$$\chi^2(d, f) = \sum_{i=1}^{T} \frac{\left\{\left(\frac{\Delta S}{S_0}\right)_i^{lab} - \left[f \times \left(\frac{\Delta S}{S_0}(d)\right)_i^{sim}\right]\right\}^2}{(\sigma_i^{lab})^2} \quad \textbf{[S7]}$$

where J_k is the kth order Bessel function of the first kind, each i corresponds to a particular value of τ, T is the number of REDOR data points, and σ^{lab} is the uncertainty of $(\Delta S/S_0)^{lab}$ (15). The fitting parameters in Eq. **S7** are d and f. Using Eq. **S5**, the σ^{lab} is calculated from σ^{exp}, the uncertainty in $(\Delta S/S_0)^{exp}$:

$$\sigma^{exp} = \frac{\sqrt{S_0^2\sigma_{S_1}^2 + S_1^2\sigma_{S_0}^2}}{S_0^2} \quad \textbf{[S8]}$$

$$\sigma^{lab} = 1.374 \times \sigma^{exp} \quad \textbf{[S9]}$$

where σ_{S0} and σ_{S1} were the experimental root-mean-square deviations of integrated intensities >1 ppm in 12 different noise regions in the S_0 and S_1 spectra (16). The parameter d in Hz can be converted to the internuclear distance r in Å of a single ^{13}CO-^{31}P or ^{13}CO-^{19}F spin pair (17):

$$d = 12250/r^3 \qquad (^{13}\text{CO-}^{31}\text{P data}) \qquad \textbf{[S10a]}$$

$$d = 28540/r^3 \qquad (^{13}\text{CO-}^{19}\text{F data}) \qquad \textbf{[S10b]}$$

Example plots of $(\Delta S/S_0)^{lab}$ and best-fit $(\Delta S/S_0)^{sim}$ vs. τ are shown in Fig. S2 and best-fit parameters are given in Table S4.

Fig. S3 shows ^{13}CO-^{31}P spectra for a sample containing HFPmn-A21 and ^{13}CO-(5-^{19}F) spectra for a sample containing HFPmn-L9. The large $(\Delta S/S_0)^{exp}$ in Fig. S3*a* indicates that the C terminus of HFPmn has close contact with ^{31}P. This conclusion was further supported by fitting of $(\Delta S/S_0)^{lab}$ to $(\Delta S/S_0)^{sim}$, Fig. S4, and may be due to Arg-22 and lysine side chains which have positive charges and which are attracted to the negatively charged phosphate groups. The full width at half maximum for the HFPmn-A21 ^{13}CO signal is ≈8 ppm, whereas the typical linewidth for residues in the Ala-1 to Ala-14 region is 3–5 ppm (Fig. 1) which probably means that the C-terminal region of HFP is less structured than the N-terminal region. In Fig. S3*b*, the ^{13}CO-(5-^{19}F) $(\Delta S/S_0)^{exp} \approx 0.3$ and should be compared with Fig. 2, which shows that for another sample containing HFPmn-L9, $(\Delta S/S_0)^{exp} \approx 0$ for the ^{13}CO-^{31}P and ^{13}CO-(16-^{19}F) data. Together with the spectra and dephasing curves shown in Fig. 5, the data support insertion of HFPmn into a single membrane leaflet (Fig. 3*B*).

1. Birdsall NJ, Lee AG, Levine YK, Metcalfe JC (1971) ^{19}F NMR of monofluorostearic acids in lecithin vesicles. *Biochim Biophys Acta* 241:693–696.
2. McDonough B, Macdonald PM, Sykes BD, McElhaney RN (1983) Fluorine-19 nuclear magnetic resonance studies of lipid fatty acyl chain order and dynamics in Acholeplasma laidlawii B membranes. A physical, biochemical, and biological evaluation of monofluoropalmitic acids as membrane probes. *Biochemistry* 22:5097–5103.
3. Sibi, MP, Rutherford, D, Sharma, R (1994) A new electrophilic alaninol synthon. A general route to oxazolidinones of D or (*R*)-2-amino alcohols from L-serine. *J Chem Soc Perkin Trans* 1:1675–1678.
4. Jackson RFW, Perez-Gonzalez M (2005) Synthesis of N-(*tert*-butoxycarbonyl)-β-iodoalanine methyl ester: A useful building block in the synthesis of nonnatural α-amino acids via palladium catalyzed cross coupling reactions. *Org Synth* 81:77–81.
5. Lang LX, Jagoda E, Ma Y, Sassaman MB, Eckelman WC (2006) Synthesis and in vivo biodistribution of F-18 labeled 3-*cis*-, 3-*trans*-, 4-*cis*-, and 4-*trans*-fluorocyclohexane derivatives of WAY 100635. *Bioorg Med Chem* 14:3737–3748.
6. Qiang W, Weliky DP (2009) HIV fusion peptide and its cross-linked oligomers: Efficient syntheses, significance of the trimer in fusion activity, correlation of β strand conformation with membrane cholesterol, and proximity to lipid headgroups. *Biochemistry* 48:289–301.
7. Yang R, Prorok M, Castellino FJ, Weliky DP (2004) A trimeric HIV-1 fusion peptide construct which does not self-associate in aqueous solution and which has 15-fold higher membrane fusion rate. *J Am Chem Soc* 126:14722–14723.
8. Qiang W, Yang J, Weliky DP (2007) Solid-state nuclear magnetic resonance measurements of HIV fusion peptide to lipid distances reveal the intimate contact of beta strand peptide with membranes and the proximity of the Ala-14-Gly-16 region with lipid headgroups. *Biochemistry* 46:4997–5008.
9. Bodner ML, et al. (2004) Temperature dependence and resonance assignment of ^{13}C NMR spectra of selectively and uniformly labeled fusion peptides associated with membranes. *Magn Reson Chem* 42:187–194.
10. Bloom M, Evans E, Mouritsen OG (1991) Physical properties of the fluid lipid-bilayer component of cell membranes: A perspective. *Quart Rev Biophys* 24:293–397.
11. Taylor KS, Lou MZ, Chin TM, Yang NC, Garavito RM (1996) A novel, multilayer structure of a helical peptide. *Protein Sci* 5:414–421.
12. Hirsh DJ, et al. (1998) A new monofluorinated phosphatidylcholine forms interdigitated bilayers. *Biophys J* 75:1858–1868.
13. Gabrys CM, et al. (2009) Nuclear magnetic resonance evidence for retention of a lamellar membrane phase with curvature in the presence of large amounts of the HIV fusion peptide. *Biochim Biophys Acta*, in press.
14. Venable RM, Brooks BR, Pastor RW (2000) Molecular dynamics simulations of gel ($L_{\beta I}$) phase lipid bilayers in constant pressure and constant surface area ensembles. *J Chem Phys* 112:4822–4832.
15. Mueller KT (1995) Analytical solutions for the time evolution of dipolar-dephasing NMR signals. *J Magn Reson Ser A* 113:81–93.
16. Bevington, PR, Robinson, DK (1992) *Data Reduction and Error Analysis for the Physical Sciences* (McGraw-Hill, Boston).
17. Schmidt-Rohr, K, Spiess, HW (1994) *Multidimensional Solid-State NMR and Polymers* (Academic, San Diego).

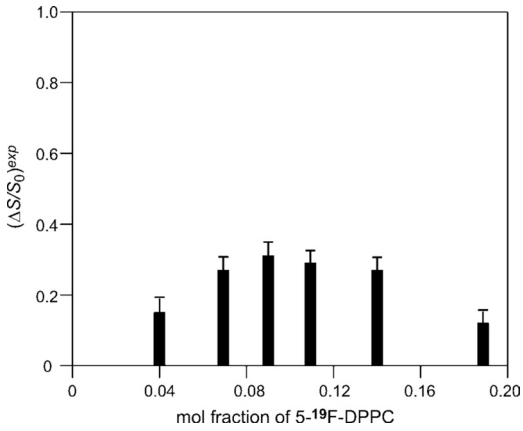

Fig. S1. Plot of ^{13}CO-^{19}F $(\Delta S/S_0)^{exp}$ vs. lipid mol fraction of 5-^{19}F-DPPC at $\tau = 16$ ms. All samples contained HFPmn-L9.

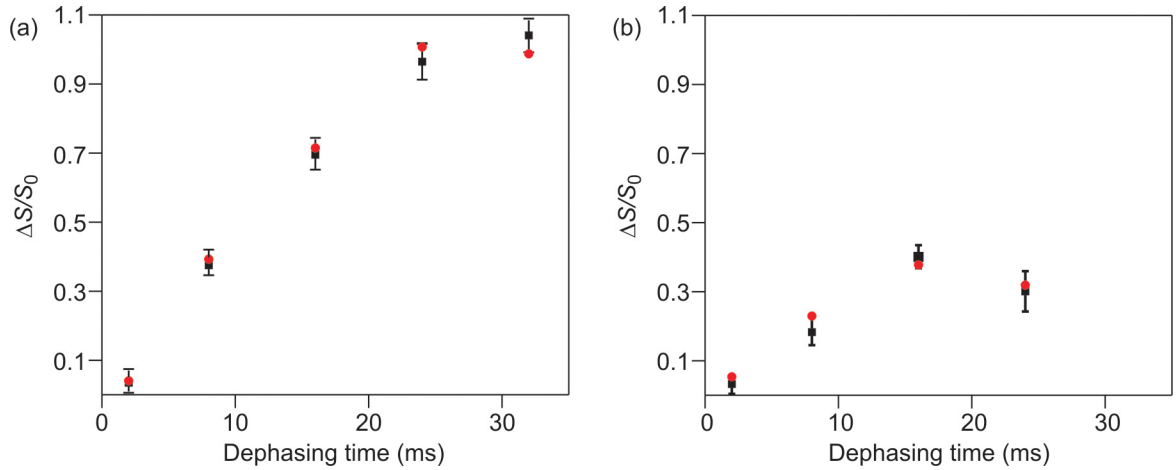

Fig. S2. Plots of $(\Delta S/S_0)^{lab}$ (black squares with error bars) and best-fit $(\Delta S/S_0)^{sim}$ (red circles) vs. dephasing time for the (*a*) ^{13}CO-^{31}P data of the sample and the (*b*) ^{13}CO-(5-^{19}F) data of the HFPmn-A6 sample. The χ^2_{min} for the best-fits were (*a*) 0.7 and (*b*) 0.5.

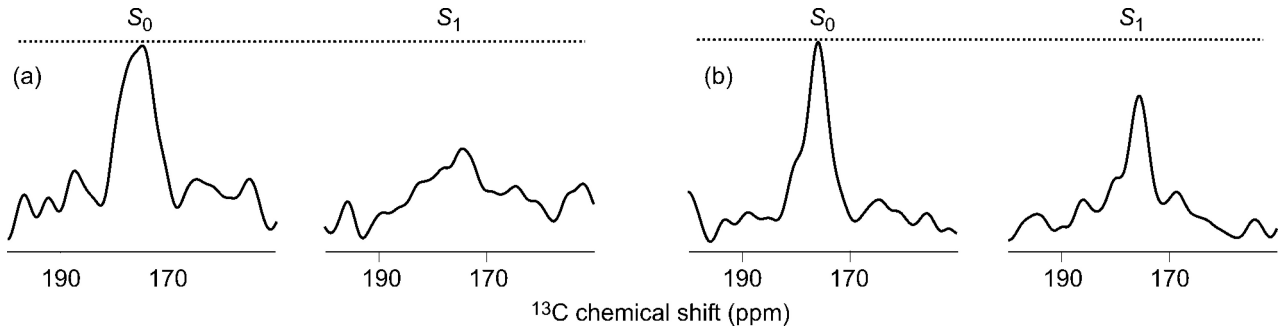

Fig. S3. (*a*) ^{13}CO-^{31}P S_0 and S_1 spectra of a sample containing HFPmn-A21 and (*b*) ^{13}CO-(5-^{19}F) spectra of a sample containing HFPmn-L9. The dephasing time was (*a*) 32 ms or (*b*) 24 ms. All spectra were processed with 200 Hz Gaussian line broadening and polynomial baseline correction. Each spectrum was the sum of (*a*) 50,000 or (*b*) 20,000 scans.

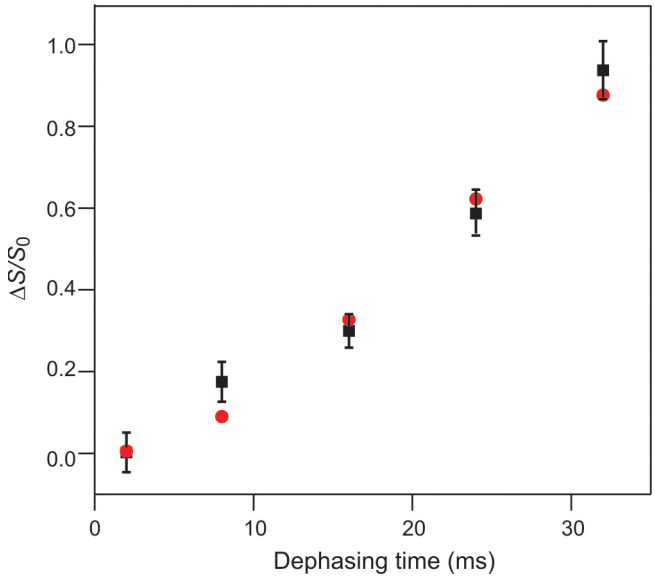

Fig. S4. ^{13}CO-^{31}P REDOR data and fitting for HFPmn-A21. For each τ, the $(\Delta S/S_0)^{lab}$ are represented by black squares with error bars and best-fit $(\Delta S/S_0)^{sim}$ are represented by red circles. The best-fit r, f, and χ^2 were 6.9 (2) Å, 0.98 (4), and 3.0, respectively.

Table S1. Peak ^{13}CO chemical shifts*†‡

Construct	Labeled residue						
	Ala1	Ile4	Ala6	Leu9	Leu12	Ala14	Ala21
HFPmn_mut	176.5	175.2	175.3	172.7	174.3	176.3	175.2
HFPmn	174.3	174.5	175.3	173.0	173.7	176.5	174.7
HFPtr	174.7	174.6	175.2	173.5	174.2	176.5	—‡

*The peak shift was measured in the ^{13}CO-^{31}P S_0 spectrum with $\tau = 2$ ms. The signal from the labeled ^{13}CO nucleus is ≈75% of the total ^{13}CO signal intensity (*SI Text*).

†The distributions of database ^{13}CO chemical shifts in β strand or helical conformation are: Ala, 176.09 ± 1.51 or 179.40 ± 1.40 ppm, respectively; Ile, 174.86 ± 1.39 or 177.72 ± 1.29 ppm; and Leu, 175.65 ± 1.47 or 178.53 ± 1.30 ppm [Zhang, HY, Neal, S, Wishart, DS (2003) RefDB: A database of uniformly referenced protein chemical shifts. *J Biomol NMR* 25:173–195].

‡HFPtr-A21 was not studied.

Table S2. The g^{na} (*HFP*)

	^{13}CO-^{31}P*			^{13}CO-(16-^{19}F)*†	^{13}CO-(5-^{19}F)*†
τ (ms)	HFPmn_mut	HFPmn	HFPtr	HFPtr	HFPmn
2	0.993	0.977	0.990	0.982	0.998
8	0.882	0.867	0.901	0.996	0.984
16	0.681	0.740	0.812	0.972	0.968
24	0.535	0.647	0.706	0.865	0.842
32	0.556	0.620	0.692	—	—

*The ^{13}CO-^{31}P values were based on the $(S_1/S_0)^{exp}$ of samples labeled at Ala1, Ile4, Ala6, Leu9, Leu12, or Ala14, and for HFPmn_mut and HFPmn, Ala21. The ^{13}CO-(16-^{19}F) values were based on samples labeled at Ala1, Ile4, Ala6, Leu9, Leu12, or Ala14 and the ^{13}CO-(5-^{19}F) values were based on samples labeled at Ala1, Ala6, or Leu9.

†The maximum τ for ^{13}CO-^{19}F experiments was 24 ms.

Table S3. The g^{na} (*DPPC*)

τ (ms)	^{13}CO-^{31}P	^{13}CO-(16-^{19}F) *	^{13}CO-(5-^{19}F) *
2	0.975	1.000	0.989
8	0.682	1.000	0.882
16	0.305	1.000	0.433
24	0.189	1.000	0.104
32	0.093	—	—

*The maximum τ for ^{13}CO-^{19}F experiments was 24 ms.

Table S4. Best-fit distance and population parameters*†‡

^{13}CO-^{31}P							
		Ala1	Ile4	Ala6	Leu9	Leu12	Ala14
HFPmn_mut	*r* (Å)	5.2 (4)	5.5 (4)	5.0 (4)	5.2 (4)	5.7 (4)	6.3 (6)
	f	0.86 (8)	0.45 (6)	0.36 (4)	0.33 (4)	0.39 (4)	0.75 (6)
HFPmn	*r* (Å)	4.8 (4)	n.d.	n.d.	n.d.	8.6 (4)	5.7 (4)
	f	0.87 (5)				0.70 (6)	0.77 (5)
HFPtr	*r* (Å)	5.1 (4)	7.9 (4)	n.d.	n.d.	9.4 (2)	5.9 (4)
	f	0.83 (7)	0.66 (6)			0.63 (6)	0.72 (6)
^{13}CO-(16-^{19}F)							
		Ala1	Ile4	Ala6	Leu9	Leu12	Ala14
HFPmn_mut	*r* (Å)	n.d.	n.d.	n.d.	n.d.	n.d.	n.d.
	f						
HFPmn	*r* (Å)	n.d.	n.d.	n.d.	n.d.	n.d.	n.d.
	f						
HFPtr	*r* (Å)	n.d.	n.d.	8.1 (6)	6.9 (4)	n.d.	n.d.
	f			0.35 (4)	0.39 (4)		
^{13}CO-(5-^{19}F)							
		Ala1	Ile4	Ala6	Leu9	Leu12	Ala14
HFPmn_mut	*r* (Å)	n.d.	—	n.d.	—	—	—
	f						
HFPmn	*r* (Å)	n.d.	—	7.0 (4)	7.3 (4)	—	—
	f			0.37 (4)	0.34 (4)		
HFPtr	*r* (Å)	n.d.	—	n.d.	—	—	—
	f						

*Best-fit *d* and *f* were determined using Eq. **S7** with typical $\chi^2_{min} < 5$. The uncertainties of *d* and *f* in parentheses were determined from the region encompassed by $\chi^2 = \chi^2_{min} + 1$ (16). The best-fit *r* and associated uncertainty was calculated with either Eqs. **S10a** or **S10b**.

†n.d. means "not determined" and refers to samples with $(\Delta S/S_0)^{exp} < 0.1$ at $\tau = 32$ ms (^{13}CO-^{31}P) or at $\tau = 24$ ms (^{13}CO-^{19}F), or to samples with no clear buildup curve.

‡A solid line means the experiment was not done.